Pergamon

Int. J. Heat Mass Transfer. Vol. 39, No. 1, pp. 81–95, 1996

0017-9310/96 $9.50+0.00

0017-9310(95)00099-2

Optimization of quench history of aluminum parts for superior mechanical properties

DAVID D. HALL and ISSAM MUDAWAR†

Boiling and Two-Phase Flow Laboratory, School of Mechanical Engineering, Purdue University, West Lafayette, IN 47907, U.S.A.

(*Received* 7 *July* 1994 *and in final form* 17 *February* 1995)

Abstract—Cooling of an age-hardenable aluminum alloy after the high temperature forming process influences the metallurgical structure and, hence, the mechanical properties of the part. An intelligent spray quenching system is proposed which selects the optimal spray nozzle configuration based on part geometry and composition such that the quenched part attains superior mechanical properties. The present study demonstrates a method for maximizing the magnitude and uniformity of hardness (and yield strength) and qualitatively minimizing residual stresses within the quenched part by manipulation of spray intensity and hydrodynamic characteristics. Furthermore, the quenching of a complex-shaped alloy with multiple, partially overlapping sprays was successfully modeled using spray heat transfer correlations as boundary conditions within a finite element program. The results of this study facilitate the eventual incorporation of optimization techniques such that the nozzle configuration for a given part can be selected prior to quenching, thus achieving superior part quality with minimal costs.

INTRODUCTION

Cost-effective fabrication of high strength aluminum alloy parts is in dire need of a systematic method for determining the appropriate production configuration. The aluminum industry reluctantly acknowledges that a large fraction of production cost is associated with post-treatment operations. Additional heat treatment or mechanical straightening of warped sections is often necessary if the product does not initially meet the required specifications. Typically, an aluminum extrusion is quenched by an array of high pressure water sprays upon exiting the extrusion die. This cooling process influences the internal microstructure of the alloy and, hence, the final metallurgical and mechanical properties. At present, choice of nozzle type, placement and operating pressure is determined from visual appearance of the part and experience of the operator. The nozzle configuration is subsequently modified until post-heat treatment tests reveal that acceptable mechanical and metallurgical properties have been obtained. An inferior quenching operation may result in parts having high residual stresses, nonuniform properties, low corrosion resistance, warping and soft spots, all of which may lead to low strength and premature part failure.

The present study is part of an ongoing research project at the Purdue University Boiling and Two-Phase Flow Laboratory, whose primary goal is the development of the CAD-based intelligent spray quenching system proposed by Deiters and Mudawar [1] and illustrated in Fig. 1. The operator enters the alloy composition and extrusion geometry into the CAD system and, upon consulting its extensive data bases, the CAD system determines the nozzle configuration (type, placement and pressure) required to achieve optimum cooling and the desired mechanical and metallurgical properties. This information is subsequently relayed to the operator or directly to an automated nozzle positioning and control system. The intelligent spray quenching system will obtain superior part quality and increase productivity by eliminating the need for costly post-treatment operations. The objective of the present study is the following: to demonstrate a method for maximizing the magnitude and uniformity of hardness and qualitatively minimizing residual stresses in heat treated Al 2024-T6 extrusions.

A successful heat treatment operation (solution heat treating, quenching and artificial aging) alters the metallurgical structure of the alloy such that acceptable mechanical properties are obtained in the final product. Figure 2(a) shows the aluminum-rich region of the aluminum–copper phase diagram and the approximate composition range of the 2××× series of aluminum alloys (indicated by the shaded region). Initially, the alloy is heated to the solution heat treatment temperature. The copper (solute) atoms completely diffuse into the aluminum (solvent) crystal lattice, forming a solid solution, when the alloy is held at this temperature for a sufficient time. Subsequent cooling causes this solid solution to become supersaturated and the alloy seeks equilibrium by precipitating the θ phase, $CuAl_2$. Slow cooling produces massive precipitation along the aluminum grain boundaries and, thus, the alloy microstructure cannot

† Author to whom correspondence should be addressed.

NOMENCLATURE

c_p	specific heat at constant pressure
C_t	critical time defined in Fig. 3(a)
d_{32}	Sauter mean diameter (SMD)
h	convection heat transfer coefficient
h_{fg}	latent heat of vaporization
H	Rockwell B hardness
k	thermal conductivity
k_1	natural logarithm of hardness ratio (or fraction of solute not precipitated) used to define the C-curve
k_j	empirical constant in the C-curve equation, $j = 2, 3, 4$, or 5
Nu_{32}	Nusselt number, $h\,d_{32}/k_f$
Pr	Prandtl number
q''	heat flux
Q''	volumetric spray flux
R	universal gas constant, 8.314 J gmol^{-1} K^{-1}
Re_{32}	Reynolds number, $\rho_f Q''\,d_{32}/\mu_f$
t	time
T	temperature
ΔT	$T_s - T_f$
ΔT_{env}	width of the temperature–time envelope at an instant in time
ΔT_{sub}	liquid subcooling, $T_{sat} - T_f$
U_m	mean drop velocity
x	coordinate along spray major axis
y	coordinate along spray minor axis.

Greek symbols

μ	dynamic viscosity
ρ	density
σ	yield strength; surface tension
τ	quench factor.

Subscripts

avg	average
c	copper heater
CHF	critical heat flux
DFB	departure from film boiling
f	saturated liquid, final condition
g	saturated vapor
i	initial condition
max	maximum
min	minimum
MIN	minimum heat flux
OSP	onset of single-phase cooling
s	surface condition
sat	saturated condition.

be enhanced by the subsequent aging process. Rapid cooling suppresses precipitation, preserving the homogeneous supersaturated solid solution, and results in an alloy that is age-hardenable and, potentially, possessing maximum strength and hardness. Figure 2(b) illustrates how artificially aging the alloy at an intermediate temperature creates a fine dispersion of precipitates within the aluminum grains. These precipitates hinder deformation of the part when it is later subjected to stress and, consequently, increase the strength and hardness of the alloy. If the precipitates begin to coalesce into a more coarse dispersion, the alloy is overaged and there will be a smaller number of dislocation barriers, thus reducing strength and hardness.

This age-hardenability viewpoint suggests cooling the entire part as quickly as possible from the solution heat treatment temperature. However, from a practical perspective, this is impossible since points on or near the quenched surface may cool much faster than locations deep within the part. Furthermore, the large spatial temperature gradients generated during a fast quench may cause non-uniform mechanical properties, high residual stresses and warping, especially in parts having a cross-section with large variations in thickness. On the other hand, a slowly quenched part

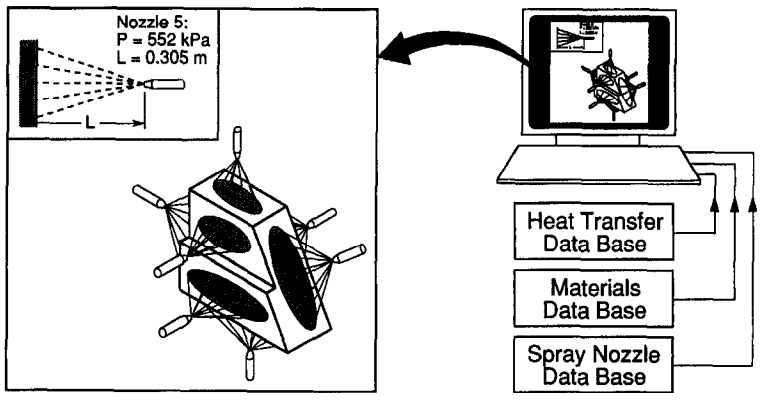

Fig. 1. CAD-based intelligent spray quenching system.

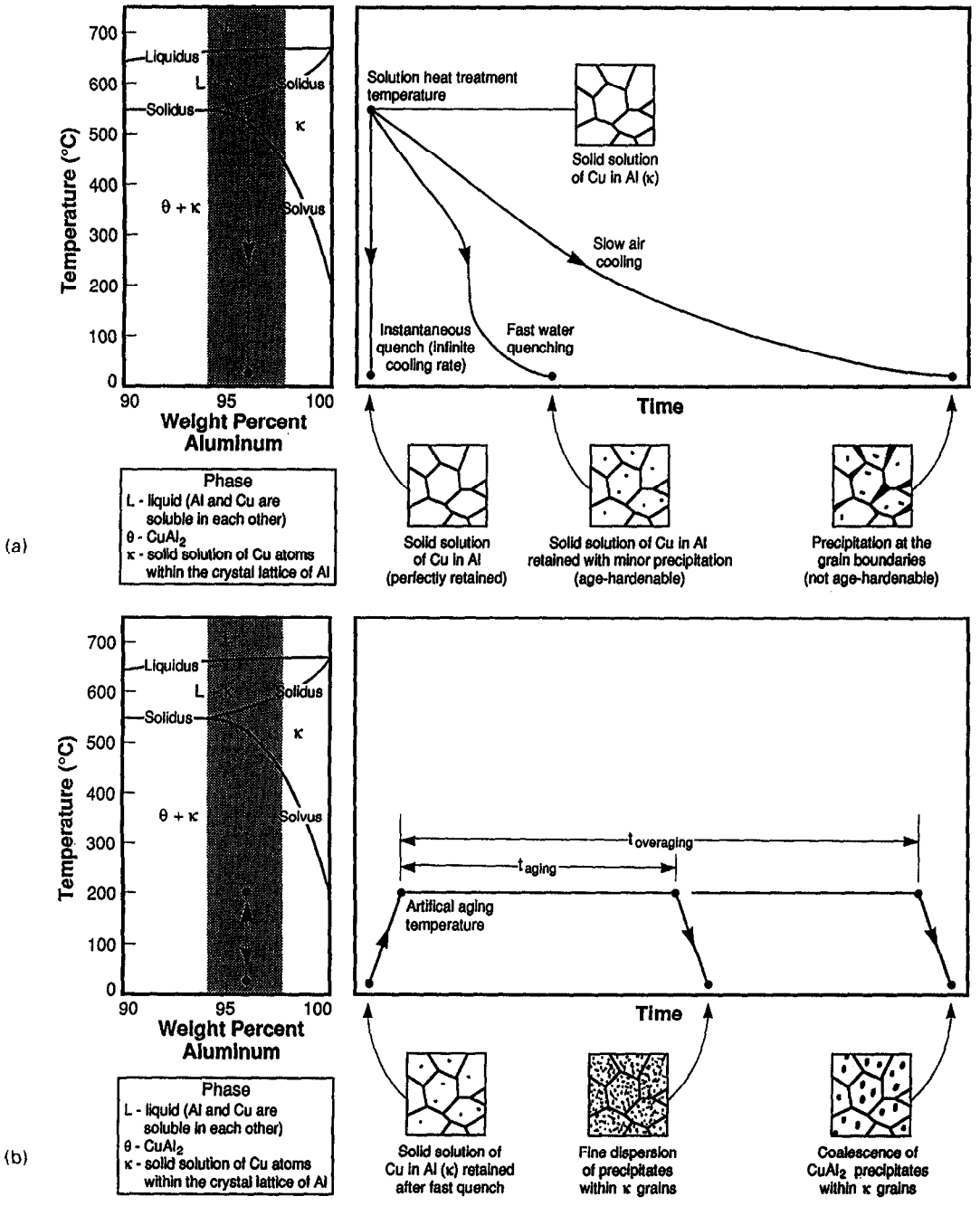

Fig. 2. Aluminum-rich region of the Al–Cu phase diagram and the microstructure that develops following (a) quenching and (b) subsequent aging of an Al–Cu (4.4 wt%) alloy.

may have uniform cooling, but the desired strength or hardness will not be obtained in the subsequent age-hardening heat treatment. Consequently, an optimum cooling strategy exists within a window of acceptable cooling rates such that the part is cooled as quickly and uniformly as possible [2]. Before this tradeoff between maximizing strength and minimizing residual stresses can be analyzed, the quality of the quenching process and its effect on mechanical properties must be quantified.

Fink and Willey [3] pioneered the attempt to describe the relationship between cooling rate (quenching rate) and final alloy strength by identifying the temperature range over which the cooling rate has its most critical influence on the mechanical properties of the aged material. Their research resulted in the development of the C-curve which represents the critical time required at different temperatures to precipitate a sufficient amount of solute to reduce the maximum attainable strength or hard-

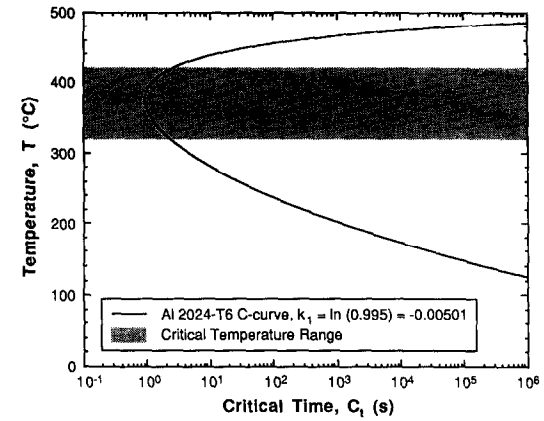

$$C_t = -k_1 k_2 \exp\left(\frac{k_3 k_4^2}{R\,T\left(k_4 - T\right)^2}\right) \exp\left(\frac{k_5}{R\,T}\right), \quad T \text{ in Kelvins}$$

(a)

Al 2024-T6 C-curve constants (Kim, 1989)	Al 2024-T6 Hardness constants (Kim, 1989)
$k_2 = 2.38 \times 10^{-12}$	$H_{max} = 78.4$ HRB
$k_3 = 1.31 \times 10^{3}$	$H_{min} = 2.2$ HRB
$k_4 = 8.40 \times 10^{2}$	
$k_5 = 1.47 \times 10^{5}$	

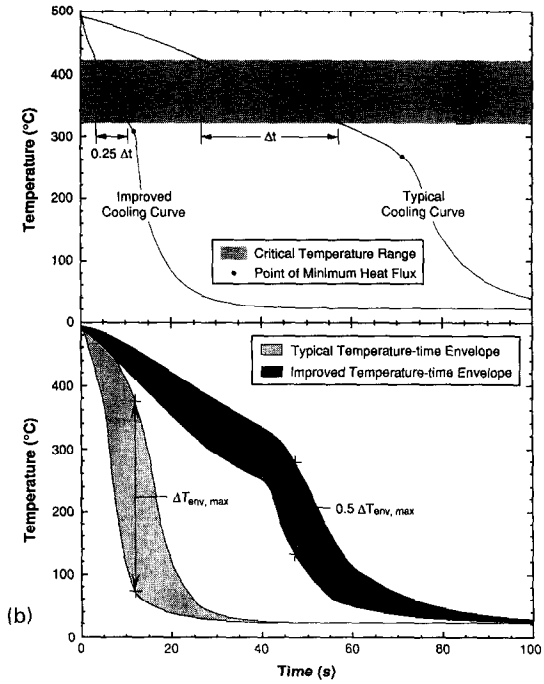

(b)

Fig. 3. (a) C-curve representing 99.5% of the maximum attainable hardness for Al 2024-T6. (b) Qualitative improvement of a quench by simultaneously increasing the cooling rate and decreasing the width of the temperature–time envelope so that hardness and yield strength are maximized while residual stresses are minimized.

ness by the percentage represented by that particular C-curve. Figure 3(a) shows the C-curve representing 99.5% of the maximum attainable hardness for Al 2024-T6 [4]. In other words, if a small Al 2024 sample were rapidly quenched from the solution heat treatment temperature to an intermediate temperature, held for the critical time, rapidly quenched to room temperature and artificially aged to achieve the T6 temper, then the resulting hardness would be 99.5% of the hardness attained if the sample were instantaneously quenched from the solution heat treatment temperature to room temperature.

During quenching, a maximum precipitation rate is obtained at intermediate temperatures, indicated by the shaded region in Fig. 3(a), where the instability of the supersaturated solid solution simultaneously causes high nucleation rates (rate at which nuclei of a critical size or larger appear) and growth rates (rate of continued precipitation at nuclei above the critical size). Fink and Willey [3] used average quenching rates through this critical temperature range to assess the quality of a quenching process. However, when cooling rates varied considerably during the quench (e.g. complex-shaped part), quantitative predictions of the final material properties using average quenching rates were not possible.

The quench factor technique developed by Evancho and Staley [5, 6] couples the time required for precipitation of the solute (i.e. C-curve) with the time available for precipitation (i.e. temperature–time cooling history of the quenched part). Cahn [7] showed that a relative measure of the amount of precipitation during a continuous cooling process is given by

$$\tau = \int_{t_i}^{t_f} \frac{\mathrm{d}t}{C_t} = \sum_{m=1}^{n} \frac{\Delta t_m}{C_{t,m}} \tag{1}$$

where τ was later referred to as the quench factor [5]. Quench factors of zero and infinity correspond to suppression of precipitation and complete precipitation, respectively. The integral in equation (1) can be calculated by discretizing the temperature–time curve into a series of small time increments (i.e. approximating an actual quench as a series of isothermal quenches), thus allowing a transient cooling process to be studied using isothermal precipitation kinetics. Each incremental quench factor represents the ratio of the amount of time the alloy was at a certain temperature to the amount of time required to obtain a specified amount of transformation at that temperature.

Since the hardness of age-hardenable aluminum alloys is proportional to strength [8, 9] and because the relative strength of age-hardenable aluminum alloys is directly related to the amount of solute remaining in solid solution after the quench [10], Evancho and Staley [5, 6] were able to use isothermal precipitation kinetics to show that

$$\frac{H - H_{min}}{H_{max} - H_{min}} = \frac{\sigma - \sigma_{min}}{\sigma_{max} - \sigma_{min}} = \exp\left(k_1 \tau\right) \tag{2}$$

where σ_{max} (or H_{max}) and σ_{min} (or H_{min}) are the maximum and minimum yield strengths (or hardness) of age-hardened specimens which have been cooled from the solution heat treatment temperature at a near infinite and extremely slow rate, respectively.

Note that k_1 in equation (2) is the natural logarithm of the hardness ratio corresponding to the C-curve from which the quench factor was calculated. Thus, given the thermal history and C-curve of an alloy, the final mechanical properties (strength or hardness) of the part can be determined using the quench factor technique. The quench factor technique has been successfully used to predict the yield strength and hardness of small (i.e. isothermal) aluminum alloy parts [4, 5, 11–14] and steel parts [15, 16].

OPTIMIZATION OF THE HEAT TREATMENT PROCESS

The intelligent spray quenching system should seek an optimum quench by minimizing the quench factor (i.e. cool the part as rapidly as possible) at all locations within the quenched part, thus obtaining a part with maximum strength and hardness. However, spatial temperature gradients present during rapid cooling promote the development of residual stresses in the following manner. Initially, the quenching process rapidly cools the surface, thus causing it to contract and impose a state of compressive stress on the interior and tensile stress on the surface. The surface layer undergoes plastic deformation when the tensile stress exceeds the local yield strength of the alloy. Then, as the interior of the part cools, it is restrained from contracting by the cooler surface material, thus placing the surface in a state of compressive stress and the interior in a state of tensile stress. When the part is completely cooled, it attains a state where the surface is under high compressive stresses balanced by tensile stresses in the interior. Consequently, the magnitudes of the residual stresses that develop in the final product and the degree of warpage or distortion that occurs during quenching tend to increase with the rate of cooling since large thermal gradients develop, especially in parts with large variations in thickness. Thus, an optimum quench must cool a part as quickly and uniformly as possible to minimize thermal gradients and still attain an acceptable strength which is uniform throughout the part cross-section.

Today, it is common practice to employ quenching configurations (e.g. bath quenching in boiling water) that provide less rapid cooling in irregular-shaped parts or parts with large cross-sections [9]. Sometimes this procedure leads to parts with an unacceptably low strength. However, high cooling rates can be maintained and fairly uniform cooling of the part can be achieved by proper location and operation of spray nozzles instead of using the more traditional bath quenching. Spray cooling allows the local surface heat flux (i.e. cooling rate) to be controlled whereas bath quenching offers no control since the entire part is constantly in contact with the coolant.

A qualitative method for minimizing the quench factor can be developed by taking the derivative of the quench factor, equation (1), with respect to temperature,

$$\frac{d\tau}{dT} = \frac{1}{C_t(dT/dt)}. \tag{3}$$

Equation (3) suggests that the quench factor can be minimized by maximizing $C_t\ dT/dt$, the product of critical time and cooling rate during the quench. At relatively high and low temperatures, the critical times are extremely large and hence cooling rate has little effect on metallurgical structure. At intermediate temperatures, the critical times are small and the cooling rates must be high, in order to increase dT/dt, if the quench factor is to be minimized, thus suppressing precipitation and maximizing strength. This critical temperature range is the same as that identified by Fink and Willey [3] in their development of the C-curve. The upper plot in Fig. 3(b) shows a typical cooling curve superimposed on the critical temperature range. While the part geometry and nozzle configuration will alter the cooling rates observed on the surface and within the quenched part, the general shape of the cooling curve will remain unchanged. By inspection, the cooling rate in the critical temperature range can be increased by increasing the film boiling heat flux and increasing the temperature of the point of minimum heat flux. Once the point of minimum heat flux is attained, the surface enters the transition boiling regime where dT/dt increases drastically. The nucleate boiling and single-phase cooling regimes appear to be of little importance to the quenching process. An improved quench curve corresponding to this discussion is also shown in Fig. 3(b).

Caution must be taken when increasing the cooling rate since this will lead to increased residual stresses, as discussed previously. The present study does not attempt to quantify residual stresses; however, a methodology was developed to minimize qualitatively the thermal gradients which lead to residual stresses. This was accomplished by minimizing the width of the temperature–time envelope of the quenched part, i.e. minimizing the temperature difference between the slowest cooling and fastest cooling locations within the part at all instants in time. Future studies will explore the complex relationship between residual stress and spatial and temporal thermal gradients. The lower plot in Fig. 3(b) shows a quench with a wide temperature–time envelope and another quench with a thin envelope. The quench with the thin envelope will result in a product with less residual stress and more uniform mechanical properties. If an active nozzle control system is used, then it may also be possible to reduce thermal gradients once portions of the part are well below the critical temperature region, which could be determined using optical radiation measurements to infer surface temperature [17]. This can be achieved by decreasing the nozzle flow rate on these areas as long as reheating back into the critical region is not allowed to occur, which would produce significantly degraded properties [12].

Obviously, the ability to predict the surface heat transfer rate of the quenched part is of utmost import-

ance if the cooling process is to be controlled to yield superior mechanical properties. Thus, spray heat transfer correlations, which relate the local heat transfer rate in each of the boiling regimes experienced by the surface to the local values of the spray hydrodynamic parameters (volumetric spray flux, mean drop diameter, mean drop velocity), were examined to gain insight into how the quenching process can be improved.

DETERMINATION OF SPRAY HEAT TRANSFER COEFFICIENTS

The quenching of aluminum alloys is usually initiated at high temperatures well above the saturation temperature of the liquid coolant. The surface experiences several distinct heat transfer regimes as the alloy cools. Initially, the surface encounters the film boiling regime, which is characterized by the formation of an insulating vapor blanket between the surface and impinging droplets, resulting in poor heat transfer. Intermittent wetting and reformation of the vapor blanket, which occurs between the point of departure from film boiling and the point of minimum heat flux, was labeled as a film wetting regime by Klinzing *et al.* [18]. As the temperature decreases below the point of minimum heat flux, the vapor blanket begins to collapse and permanent, partial wetting of the surface occurs. This transition boiling regime is marked by a significant increase in the surface heat flux due to local areas of intense boiling, thus causing a rapid decrease in surface temperature. The vapor layer virtually vanishes at the point of critical heat flux (CHF) and cooling rates remain fairly high in the ensuing nucleate boiling regime as the entire surface experiences liquid contact. Boiling completely subsides in the single-phase cooling regime and the relatively low heat transfer rate is simply due to forced convection with the impinging liquid.

A series of studies on heat transfer from hot metallic surfaces to water sprays was performed at the Purdue University Boiling and Two-Phase Flow Laboratory [18, 19]. This research culminated in heat transfer correlations applicable to industrial sprays commonly employed in materials processing. The methodology utilized to develop these correlations is discussed below in an effort to ascertain the effect of the spray hydrodynamic parameters on the spatial distribution of the heat transfer coefficient.

Spray hydrodynamic parameters

Mudawar and Valentine [19] conducted a comprehensive literature review and concluded that sprays could be characterized in terms of the distribution of spray hydrodynamic parameters (volumetric spray flux, mean drop diameter and mean drop velocity) just prior to impingement upon the surface. The volumetric spray flux, Q'', is defined as the local volume flow rate per unit surface area. Sauter mean diameter, SMD or d_{32}, is the diameter of the drop whose ratio of volume to surface area is the same as that of the entire measurement sample. The mean drop velocity, U_m, is simply the average of measured individual drop velocities. Accurate knowledge of the spatial distribution of the spray hydrodynamic parameters is essential if the spray quenching process is to be numerically modeled, therefore the spray hydrodynamic parameters were measured at discrete locations within the spray field using the techniques described in ref. [20]. Table 1 summarizes the spatial distribution models of the spray hydrodynamic parameters for the flat spray nozzles used in the present study. A repeatability study was also conducted to verify that the models developed using a single nozzle were applicable to all nozzles of that type.

Steady state measurement technique

Mudawar and Valentine [19] constructed the copper heater in Fig. 4(a) which was used in the present studies to measure local heat transfer rates within a spray field. High purity copper was utilized since it was more resistant to oxidation than aluminum and, hence, capable of prolonged high temperature operation. Heat was supplied to an instrumented calorimeter bar by nine cartridge heaters. The small cross-sectional area of the calorimeter bar (0.5 cm^2) allowed the detection of sharp spatial gradients in the heat transfer coefficient within the spray field. The heater and calorimeter section were surrounded with insulation to ensure parallel heat flow lines through the thermocouple region. The spray cooling process was initiated by engaging the pump within the fluid delivery loop and allowing the downward impinging spray to reach hydrodynamic equilibrium. The exposed surface of the heater was positioned at the center of the spray field. The heat flux at steady state was determined from the uniform temperature gradient between the thermocouples placed along the axis of the calorimeter bar. The linear temperature distribution was extrapolated to the surface to obtain the steady state surface temperature. The input power was subsequently increased in small increments so that a nearly continuous boiling curve was obtained upon processing of the data.

Seven stainless steel full cone and flat spray nozzles were operated at various nozzle-to-surface distances and inlet pressures to obtain a wide range of the spray hydrodynamic parameters. Figure 4(b) shows various boiling curves obtained using the steady state measurement technique. Volumetric spray flux was found to have a dominant effect on heat transfer compared with the other hydrodynamic parameters, especially in the single-phase regime where an increase in volumetric spray flux yielded a noticeable increase in surface heat flux. Heat transfer in the nucleate boiling regime was insensitive to the spray hydrodynamic parameters. Heat transfer correlations based on surface temperature, fluid properties, and the local spray hydrodynamic parameters were developed for the nucleate boiling and single-phase cooling regimes, as

Table 1. Spatial distribution models of the spray hydrodynamic parameters for the flat spray nozzles

Nozzle type	Pressure [kPa (psig)]	Distance [m (in)]	Flow rate [$m^3 s^{-1} \times 10^6$ (gpm)]	$d_{32} \times 10^6$ [m]	U_m [$m s^{-1}$]	$Q''(x, y)$† [$m^3 s^{-1} m^{-2}$]
A	138 (20)	0.305 (12.0)	8.8 (0.14)	463	9.6	$Q'' = 2.63 \times 10^{-3} \exp(-163x^2 - 1130y^2)$
A	552 (80)	0.305 (12.0)	18 (0.28)	286	13.5	$Q'' = 4.24 \times 10^{-3} \exp(-143x^2 - 3790y^2)$
B	552 (80)	0.305 (12.0)	36 (0.57)	320	15.8	$Q'' = 9.91 \times 10^{-3} \exp(-134x^2 - 5470y^2)$
C	552 (80)	0.305 (12.0)	69 (1.1)	354	18.0	$Q'' = 21.4 \times 10^{-3} \exp(-123x^2 - 5120y^2)$

† The coordinates x and y, shown in the $Q''(x, y)$ equations, have units of meters.

well as the points of critical heat flux and incipient boiling (onset of single-phase cooling). These correlations, listed in Table 2, are universal to all spray types provided that the local spray hydrodynamic parameters are within the given limits. The transition to film boiling was unsteady and, hence, an alternative method was required to characterize these high temperature boiling regimes.

Transient measurement technique

Klinzing *et al.* [18] developed a technique for extracting the surface heat flux from the transient temperature history of a quenched disk. A thin copper disk having an exposed surface area of 0.5 cm^2 was embedded in an insulating casing as shown in Fig. 5(a). Temperature was measured using a chromel–alumel thermocouple spot welded to the disk underside. The disk was preheated to an initial temperature of 530°C using an oxyacetylene torch. Once the spray reached hydrodynamic equilibrium, the torch was removed and the spray was allowed to contact the disk. Using the lumped capacitance method, the disk temperature was assumed to be uniform and equal to that recorded by the thermocouple at every instant during the quench. Figure 5(b) shows temperature–time histories of the copper disk for increasing volumetric spray flux.

From the measured temperature response, the instantaneous surface heat flux was determined by solving the transient heat diffusion equation for a lumped mass. Correlations for the film boiling regime, point of departure from film boiling and point of minimum heat flux were formulated from the boiling curves shown in Fig. 5(c). The nucleate boiling and single-phase cooling regimes could not be characterized using the transient measurement technique since the relatively high heat transfer coefficient violated the lumped mass approximation. The heat flux correlations for the film wetting and transition boiling regimes were chosen to be polynomial functions of ΔT. The unknown constants were determined by forcing the curve-fits to yield a maximum heat flux at CHF and a minimum at the point of minimum heat flux. Furthermore, continuity of heat flux was required at the transitions between boiling regimes. Spray quenching heat transfer correlations developed using these techniques are listed in Table 2.

Impact of the spray quenching heat transfer correlations on the optimization process

The spray quenching heat transfer correlations shown in Table 2 give an insight into how to accelerate (or decelerate) the cooling process (i.e. local surface cooling rate) to achieve higher hardness and strength. A general examination yields the following guidelines:

(1) The film boiling heat flux can be increased by increasing the volumetric spray flux (film boiling heat flux is relatively insensitive to drop diameter and velocity). The minimum heat flux and departure from film boiling temperatures can both be increased by increasing the mean drop velocity and, to a lesser extent, the volumetric spray flux.

(2) The local volumetric spray flux and mean drop velocity can both be increased by either: (i) increasing the nozzle operating pressure; or (ii) using a nozzle with a larger flow capacity.

(3) The major advantage of spray quenching over bath quenching is that cooling can be locally controlled by applying heavy sprays to areas of the part where higher surface cooling rates are required and applying lighter sprays to areas of relatively lower thermal mass such that the entire part cools as quickly and uniformly as possible.

(4) The correlations are also an invaluable tool for predicting the temperature response of quenched parts. Once the effect of spray interaction is accounted for, the correlations can be used as boundary conditions in a numerical analysis of the quenching process.

EXPERIMENTAL VERIFICATION TECHNIQUE

An A1 2024 extrusion, which was obtained from the Aluminum Company of America (ALCOA), was machined into the L-shaped testpiece shown in Fig. 6(a). The thick and thin protruding sections, which had a thermal mass ratio of 4:1, facilitated the investigation of section thickness and spray configuration on cooling uniformity. As shown Fig. 6(a), 10 chro-

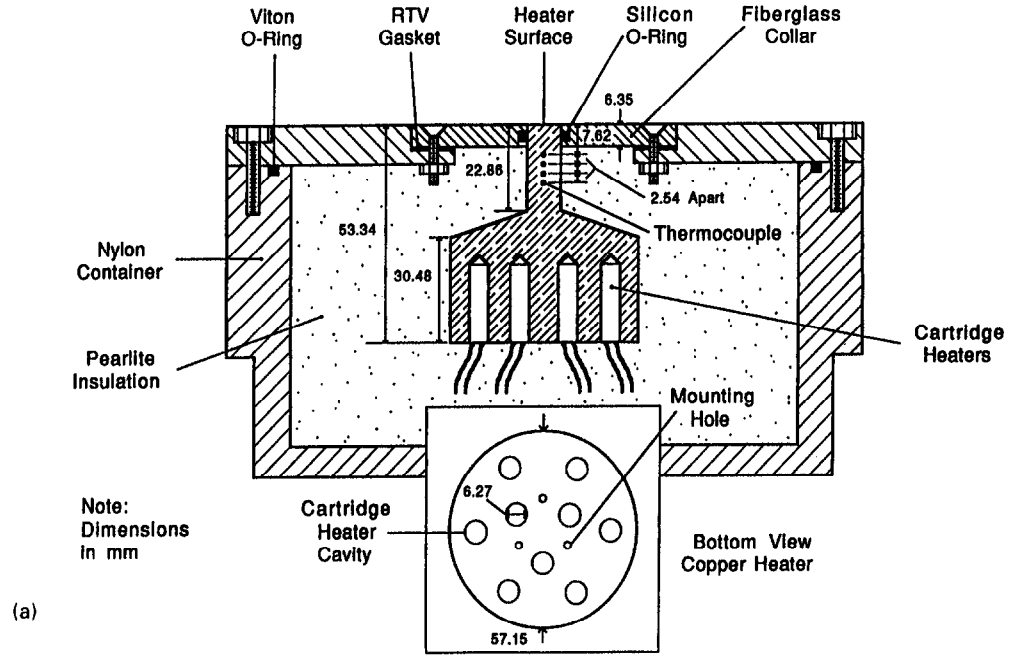

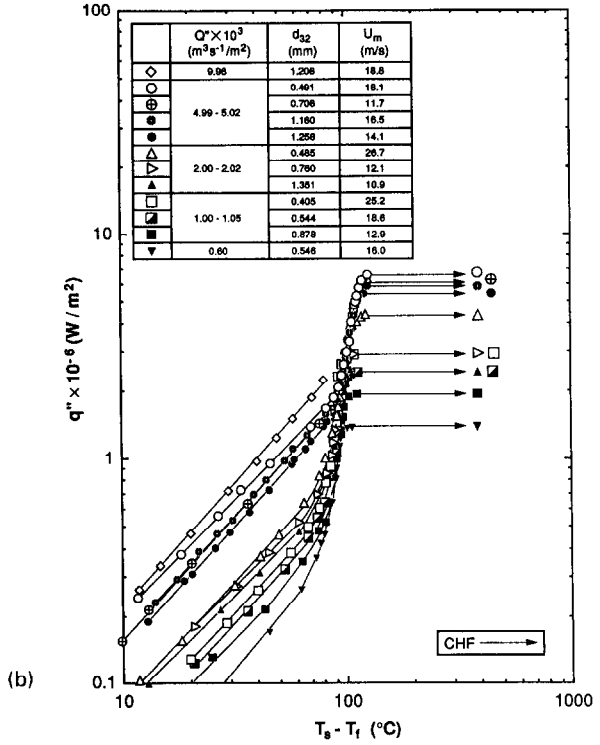

Fig. 4. (a) Steady state heater schematic and (b) spray boiling curves.

mel–alumel (type K) thermocouples, which consisted of 0.13 mm (0.005 in) wire within a 0.81 mm (0.032 in) diameter Inconel 600 sheathing with magnesium oxide insulation, were located in a plane one-fourth the length of the L-shape above the lower surface. Boron nitride powder was used to fill the void surrounding the thermocouple bead since, unlike air, it has a thermal conductivity comparable with aluminum. The repeated quenching of a part was observed to alter the surface characteristics and, hence, thermal history of the part [21]. Furthermore, the spray quenching heat transfer correlations used to predict the thermal history were developed using polished surfaces [18, 19]. Thus, the testpiece surface was polished before each test to ensure uniform surface roughness and repeatability between quenches.

Table 2. Spray quenching heat transfer correlations

Quenching (boiling) regime	Correlation
Film boiling regime [18]	$q'' = 6.325\times10^{1}\Delta T^{1.691}Q''^{0.264}d_{32}^{-0.062}$
Point of departure from film boiling [18]	$q''_{DFB} = 6.100\times10^{6}Q''^{0.588}U_m^{0.244}$
	$\Delta T_{DFB} = 2.808\times10^{2}Q''^{0.087}U_m^{0.110}d_{32}^{-0.035}$
Film-wetting regime [18]	$q'' = q''_{MIN} + (q''_{DFB} - q''_{MIN})\left(\frac{\Delta T-\Delta T_{MIN}}{\Delta T_{DFB}-\Delta T_{MIN}}\right)^2$
Point of minimum heat flux [18]	$q''_{MIN} = 3.324\times10^{6}Q''^{0.544}U_m^{0.324}$
	$\Delta T_{MIN} = 2.049\times10^{2}Q''^{0.066}U_m^{0.138}d_{32}^{-0.035}$
Transition boiling regime [18]	$q'' = q''_{CHF} - \frac{q''_{CHF}-q''_{MIN}}{(\Delta T_{CHF}-\Delta T_{MIN})^3}[\Delta T_{CHF}^3 - 3\Delta T_{CHF}^2\Delta T_{MIN} + 6\Delta T_{CHF}\Delta T_{MIN}\Delta T - 3(\Delta T_{CHF}+\Delta T_{MIN})\Delta T^2 + 2\Delta T^3]$
Point of critical heat flux [19]	$\frac{q''_{CHF}}{\rho_g h_{fg} Q''} = 122.4\left[1+0.0118\left(\frac{\rho_g}{\rho_f}\right)^{1/4}\left(\frac{\rho_f c_{p,f}\Delta T_{sub}}{\rho_g h_{fg}}\right)\right]\left(\frac{\sigma}{\rho_f Q''^2 d_{32}}\right)^{0.198}$
	$\Delta T_{CHF} = 18.0\left[(\rho_g h_{fg} Q'')\left(\frac{\sigma}{\rho_f Q''^2 d_{32}}\right)^{0.198}\right]^{1/5.55}$
Nucleate boiling regime [19]	$q'' = 1.87\times10^{-5}(\Delta T)^{5.55}$
Onset of single-phase cooling [19]	$\Delta T_{OSP} = 13.43 Re_{32}^{0.167} Pr_f^{0.123}\left(\frac{k_f}{d_{32}}\right)^{0.220}$
Single-phase regime [19]	$Nu_{32} = 2.512 Re_{32}^{0.76} Pr_f^{0.56}$

Units of the parameters: q'' [W m^{-2}], $\Delta T = T_s - T_f$ [°C], Q''[m^3 s^{-1} m^{-2}], U_m[m s^{-1}], d_{32}[m], h[W m^{-2} K^{-1}], ρ_f[kg m^{-3}], ρ_g[kg m^{-3}], h_{fg}[J kg^{-1}], $c_{p,f}$[J kg^{-1} K^{-1}], k_f[W m^{-1} K^{-1}], μ_f[N s m^{-2}], σ[N m^{-1}].

Dimensionless parameters: $Nu_{32} = h\,d_{32}/k_f$, $Pr_f = c_{p,f}\mu_f/k_f$, $Re_{32} = \rho_f Q'' d_{32}/\mu_f$.

Range of validity of the correlations: $T_f = 23$°C, $Q'' = 0.58\times10^{-3}$–9.96×10^{-3} m^3 s^{-1} m^{-2}, $U_m = 10.1$–29.9 m s^{-1}, $d_{32} = 0.137\times10^{-3}$–$1.35\times10^{-3}$ m.

Properties: the fluid properties used in the correlations for the point of incipient boiling and the single-phase regime are evaluated at the film temperature, $T_{film} = 0.5\,(T_s + T_f)$. The fluid properties used in the CHF correlation are evaluated at the fluid saturation temperature [19].

A materials processing test bed was used to simulate the heat treatment process (solution heat treating, spray quenching and artificial aging) of aluminum alloys in an industrial environment. Figure 7 shows a schematic containing the major components (furnace, translation system, spray chamber, quench tank, external plumbing, and data acquisition and processing system) of the facility. The testpiece was heated in a Lindberg model 54857-V tube furnace having a cylindrical heating length of 60 cm and diameter of 15 cm. The vertical translation system lowered the testpiece from the furnace mounted above the quench tank into the spray chamber. The spray chamber was fabricated from optical grade Lexan sheet to allow visual access to the quenching process. An exhaust system connected to the back of the facility removed steam produced during the quench. A fan-cooled centrifugal pump, rated to deliver 25.2×10^{-3} m^3 s^{-1} (40 gpm) at 690 kPa (100 psi), circulated water contained in the lower quench tank. A 5 μm filter removed impurities from the water which could possibly accumulate near the nozzle orifice and cause flow blockage. The bypass line back into the quench tank was required to maintain flow stability. An independently controlled nozzle array was mounted on each side of the spray chamber. Each nozzle array consisted of three spray nozzles vertically separated by 11.4 cm (4.5 in). The nozzle arrays allowed some flexible positioning relative to the testpiece; however, the configuration shown in Fig. 6(b) was used for all tests conducted in this study.

The experiment began when the testpiece was raised into the furnace using the vertical translation system. Once the testpiece attained the solution heat treatment temperature (495°C for Al 2024), the quenching process was initiated by engaging the pump and allowing the sprays to reach hydrodynamic equilibrium. The operating pressure of each nozzle array was monitored using glycerin filled stainless steel pressure gages with a range of 0–1.10 MPa (0–160 psi). The testpiece was quickly lowered into the spray chamber using the translation system and the output of the thermocouples was recorded every 0.1 s during the quench.

RESULTS AND DISCUSSION

Spray quenching tests were conducted using the materials processing test bed in order to investigate

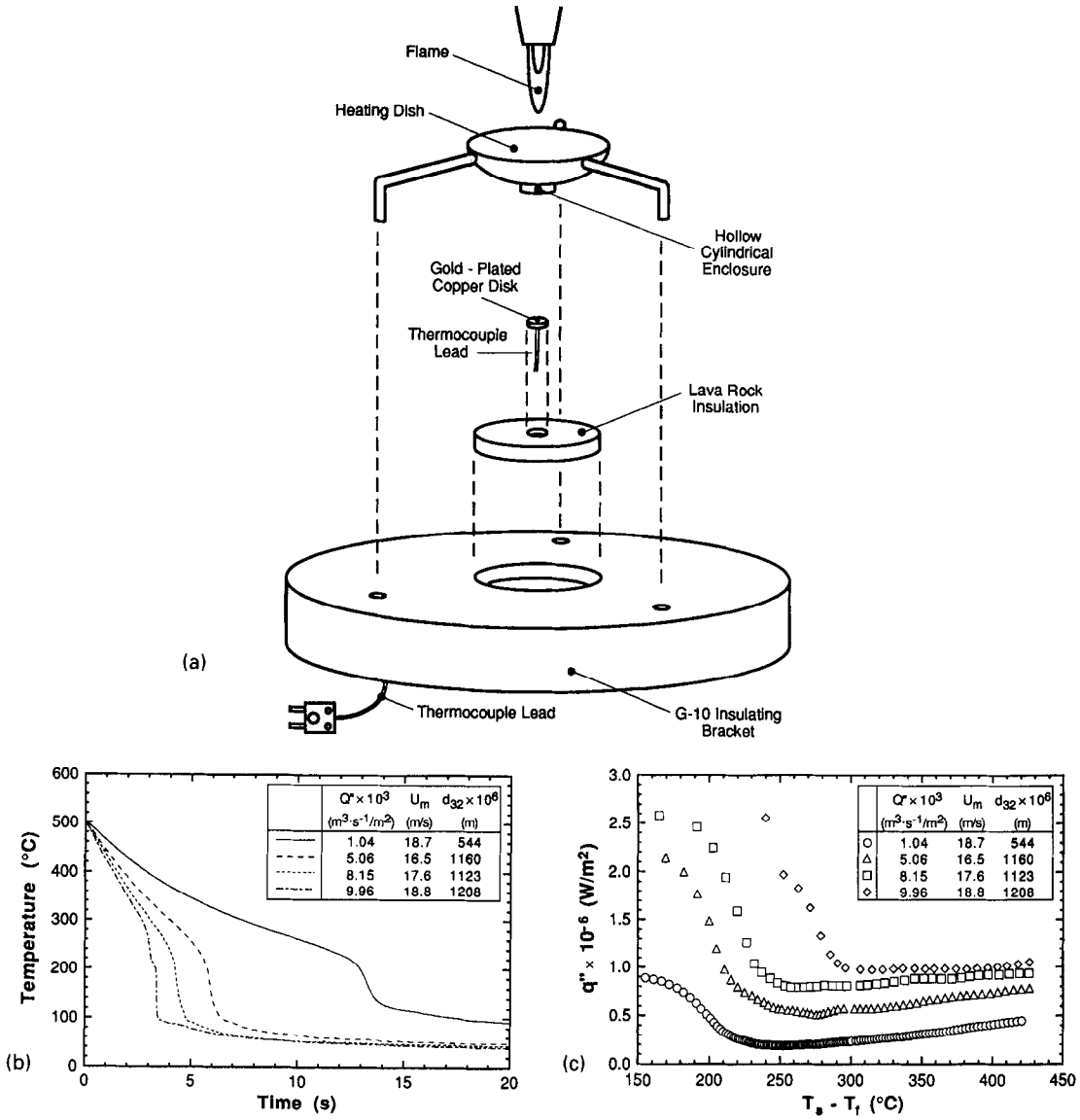

Fig. 5. (a) Schematic of copper disk assembly. Variation of (b) temperature response and (c) boiling curve of the copper disk with increasing volumetric spray flux.

experimentally the effect of nozzle configuration on the cooling history of the L-shape. The temperature–time envelope of each test is presented to allow determination of the maximum temperature difference within the part during the quench, thereby providing a qualitative indication of the residual stress distribution within the part. Also, the quench factor technique was used to predict the hardness distribution which would develop in an identical testpiece following a complete heat treatment. Furthermore, a series of tests were performed on the L-shape to demonstrate that a nozzle configuration exists which optimizes the resulting mechanical properties of the part (i.e. maximizes the magnitude and uniformity of hardness and minimizes the temperature-time envelope). The ability to predict the temperature–time envelope for a given part and nozzle configuration was also demonstrated.

Trends in quench rate and temperature–time envelope

The top plot in Fig. 8 shows the temperature–time envelope of the L-shape for a quench using type A nozzles operating at a pressure of 138 kPa (20 psig) in the four nozzle arrays illustrated in Fig. 6(b). The complete temperature–time history of four thermocouples is presented. The temperature–time curves of the remaining six thermocouples are omitted for clarity. TC 5, which is located in the center of the thick section, cooled the slowest due to the relatively large thermal mass surrounding the thermocouple. In contrast TC 9, which is located near the surface of the thin section close to the major axis of a nozzle array, cooled the

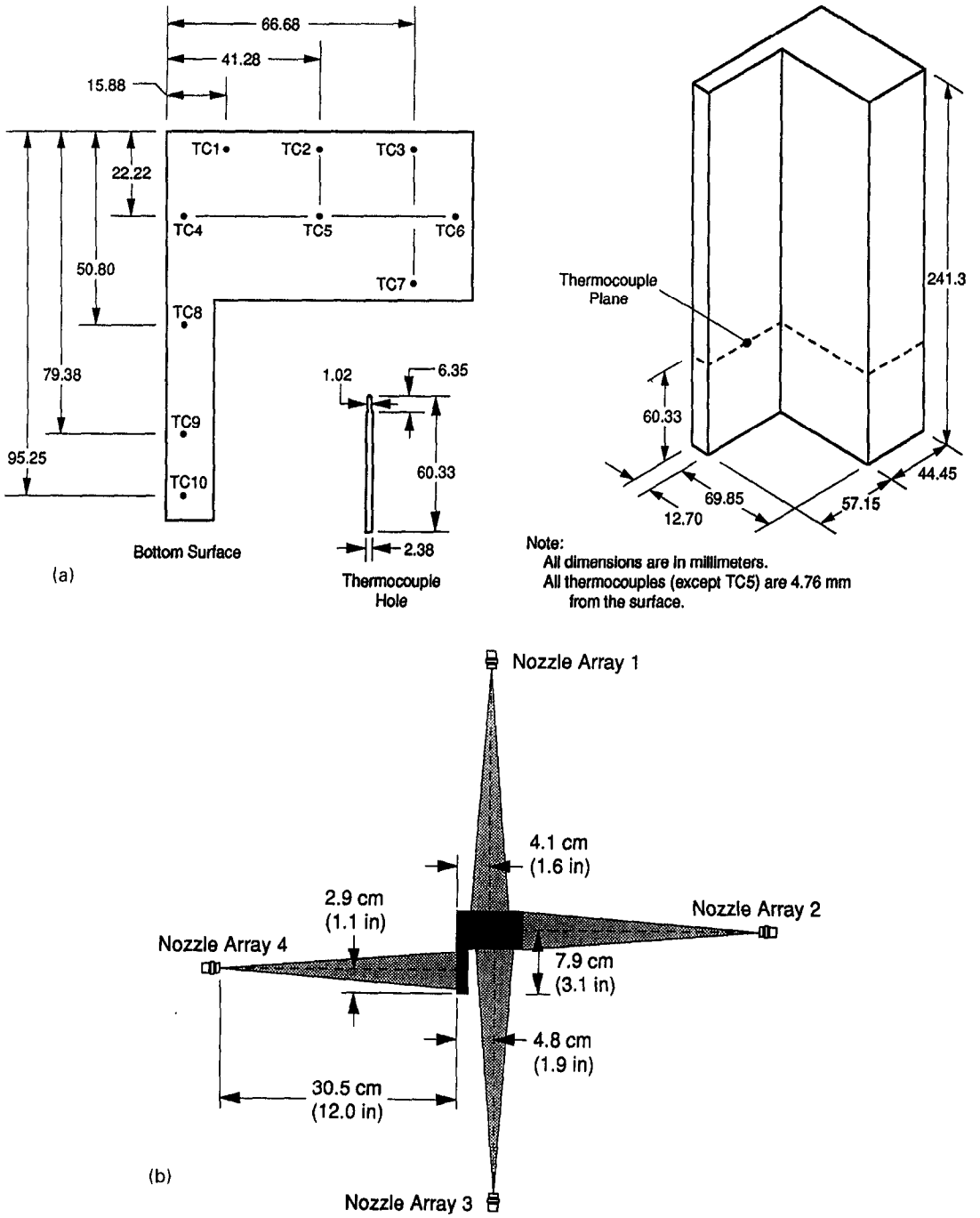

Fig. 6. (a) Al 2024 L-shape dimensions and thermocouple placement and (b) nozzle configuration used in the present study.

fastest owing to the relatively low thermal mass of the thin section. The point of minimum heat flux for a thermocouple near a sprayed surface (TC 6 and TC 9) is readily identified as the point at which the cooling curve has an abrupt change in slope. When a sprayed surface enters the transition boiling regime, the surface experiences a large drop in temperature which is quickly sensed by interior locations. This phenomenon is responsible for the corresponding change in slope of TC 5 which occurred a short time after TC 6 entered the transition boiling regime. This time delay is noticeable because of the large thermal mass of the thick section. The maximum width of the temperature–time envelope, $\Delta T_{\text{env,max}}$, occurred when the sprayed surface of the thin section (see TC 9) entered the single-phase cooling regime as the center of the thick section (see TC 5) began to experience the effect of nearby surfaces entering the transition boiling regime.

Figure 8 also illustrates temperature–time envel-

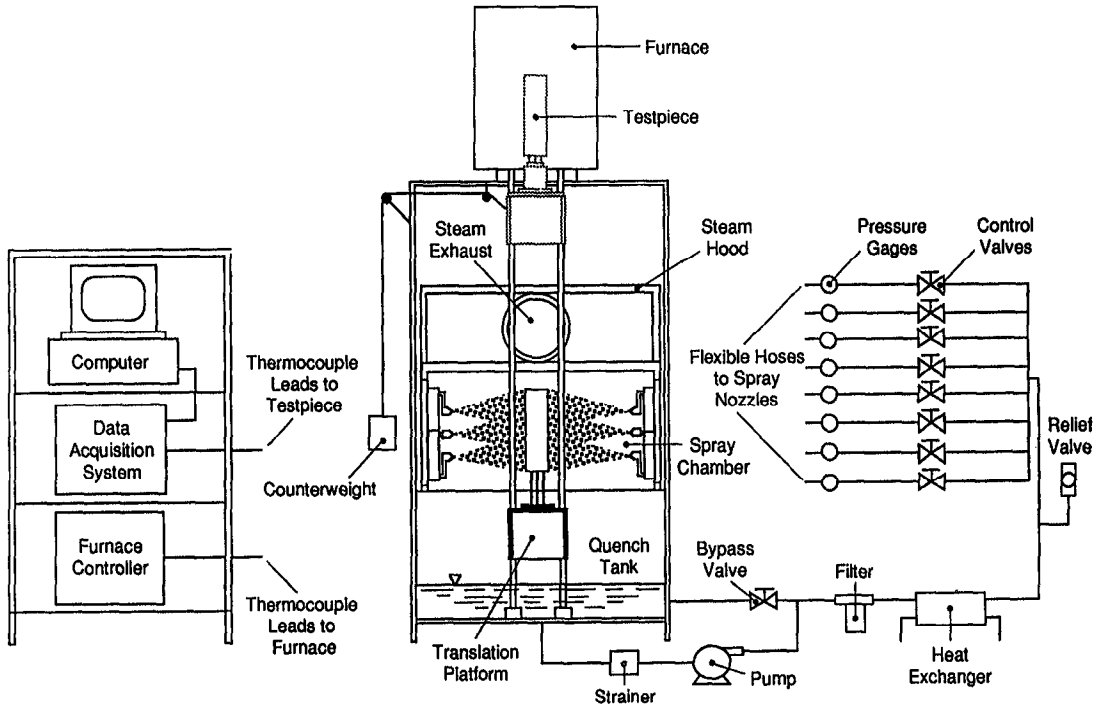

Fig. 7. Schematic of the materials processing test bed.

opes of the L-shape for quenches using either nozzle types A, B or C operating at pressures of 552 kPa (80 psig) in all four nozzle arrays. At this pressure, nozzles B and C have flow rates of two and four times the flow rate of nozzle A, respectively. The cooling trends observed in these cases are similar to those discussed in the previous paragraph. In general, a quench using four nozzle arrays all having nozzles of the same type has a temperature–time envelope bounded by TC 5 (thick section) and TC 9 (thin section). The L-shape cools quicker as the flow rate of the impinging fluid is increased (see Table 1 for nozzle specifications). Note that the volumetric spray flux, which is directly related to the nozzle flow rate, is the controlling factor for the local convection heat transfer coefficient in the film boiling and transition boiling regimes (see Table 2). The quench using type C nozzles, despite its superior cooling effectiveness relative to nozzle types A or B, has the largest value of $\Delta T_{\text{env,max}}$ and, hence, is expected to have the largest amount of residual stress remaining in the part after the heat treatment process. This is proof that achieving a faster quench, in order to increase hardness and strength, is often realized at the expense of greater residual stresses. The relatively large volumetric spray flux associated with nozzle type C causes the film boiling heat flux to be comparable with the transition boiling heat flux. One plausible explanation is that the vapor layer characteristic of the film boiling regime is being continuously disrupted by a high spray flux of relatively large, fast moving droplets and, therefore, the change in slope of the cooling curve at the point of minimum heat flux is barely noticeable.

At each thermocouple location, the quench factor technique was applied to the temperature measurements to predict hardness. The maximum, average, and minimum predicted hardness, obtained using equations (1) and (2) along with the measured temperature–time history, for the quenching experiments presented in Fig. 8, are shown to the immediate right of each individual plot. As the nozzle flow rate of the quench was increased, the quench factor technique predicted an increase in hardness; however, experimental measurements (Fig. 8) also showed that thermal gradients within the part increased, leading to potentially higher residual stresses. Thus, a tradeoff exists between maximizing hardness and minimizing residual stress.

Quench improvement experiments

By choosing a more appropriate nozzle configuration it should be possible to lower the thermal gradients present in a previous test while still maintaining relatively high hardness. The initial nozzle configuration chosen by both experience and intuition consisted of nozzle array one (type A nozzles operated at 552 kPa) impinging upon the thick section only (i.e. with nozzle arrays two, three and four turned off). The resulting temperature–time envelope is the uppermost plot displayed in Fig. 9. TC 2 cooled fastest because it was located near the surface of the thick section at the major axis of the only operational nozzle array. The absence of sprays on the thin section caused it to cool relatively slow as evidenced by TC 10. This quench had unacceptably low hardness and high thermal gradients. A first attempt to correct this problem

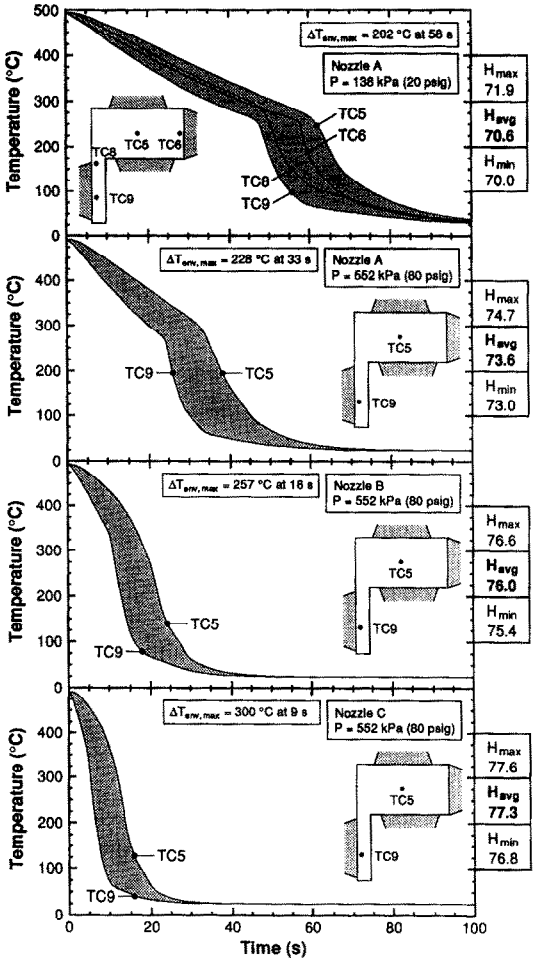

Fig. 8. Temperature–time envelopes of the L-shape for a series of quench experiments with various nozzle types.

consisted of applying an additional light spray (type A nozzles operated 138 kPa) to the thin section (nozzle array four), the second plot from the top in Fig. 9. The overall hardness is still lower than the quenches shown in Fig. 8. Further attempts at improving the quench and resulting mechanical properties should consist of increasing the cooling rate of the slowest cooling areas of the part. Thus, a spray should be applied to a surface near TC 7 to increase the cooling rate of the surrounding area. The third plot in Fig. 9 shows the temperature–time envelope produced by the addition of nozzle array three with type A nozzles at 552 kPa (80 psig). The thermal gradients have been significantly reduced and hardness increased relative to the previous quench. A final attempt at increasing the magnitude and uniformity of hardness while maintaining the same value of $\Delta T_{\text{env,max}}$ is the lower plot in Fig. 9. The replacement of type A nozzles with type B nozzles in nozzle array one caused the cooling rates of the thick and thin sections to become nearly identical. TC 4, which was near an unsprayed surface and in neither of the two protruding sections of the L-shape, cooled the slowest while TC 2 cooled quickest. TC 2 was in close proximity to TC 4, but it was near the surface of the thick section at the major axis of nozzle array one. This last quench achieved a relatively high uniform hardness distribution while maintaining low thermal gradients. Note that the quench factor technique predicted the fastest cooling thermocouple, TC 2 (73.1 Rockwell B hardness), to have a hardness lower than the slowest cooling thermocouple, TC 4 (73.9 Rockwell B hardness). This phenomenon occurred because TC 4 spent less time than TC 2 within the critical temperature range where precipitation rates are highest (320–420°C). Figure 10 compares the temperature–time envelope of the final improved quench with the initial quench on an expanded time scale. The average hardness of the part was increased by 14% while the maximum width of the temperature–time envelope was reduced by 33%. These effects would be more pronounced for parts having cross-sections with larger variations in thickness.

Numerical prediction of thermal history

These spray quenching tests prove that it is possible to improve the quench history of a part using exper-

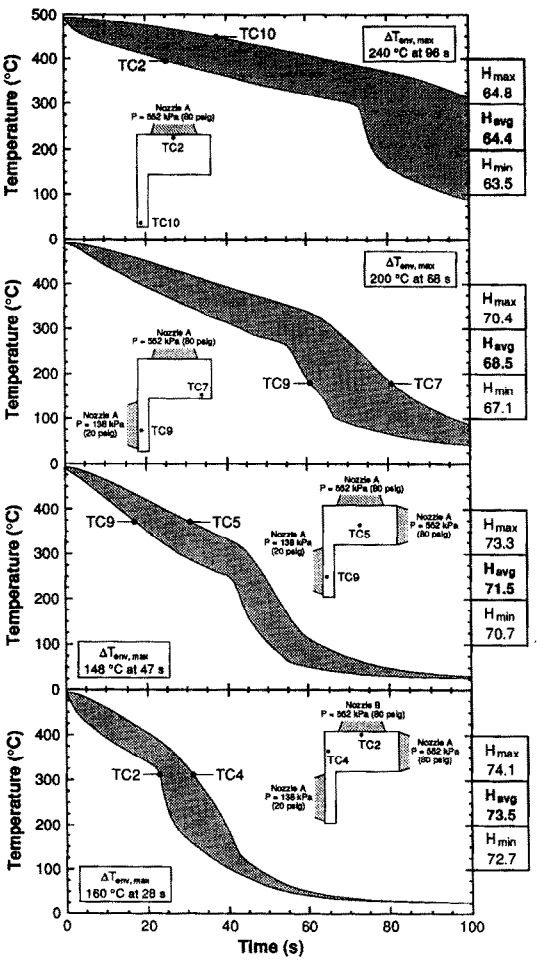

Fig. 9. Temperature–time envelopes of the L-shape for the series of quench improvement experiments.

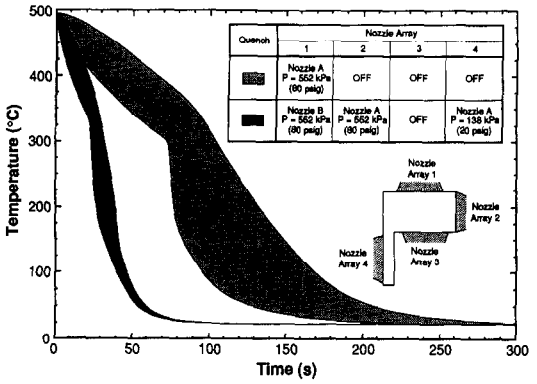

Fig. 10. Comparison of the temperature–time envelopes of the L-shape for a poor quench and an improved quench.

imental data and the intuition of the operator. The objective of the proposed CAD-based intelligent spray quenching system is to accomplish this series of experiments numerically, thus eliminating the need for a trial and error procedure of changing the nozzle configuration until the desired mechanical properties have been attained. The thermal history of a complex-shaped part quenched with multiple, partially overlapping sprays was predicted by using the finite element method to solve the transient heat diffusion equation with temperature and spatially dependent boundary conditions. The spray quenching heat transfer correlations shown in Table 2 were used to define the heat transfer coefficient as a function of surface temperature and the local spray hydrodynamic parameters. A method was developed for modifying the spatial distribution models of the spray hydrodynamic parameters to account for the effect of spray interaction between adjacent nozzles [20]. Figure 11 presents quenches using all nozzle arrays and either type A or B nozzles. In both cases, the temperature–time

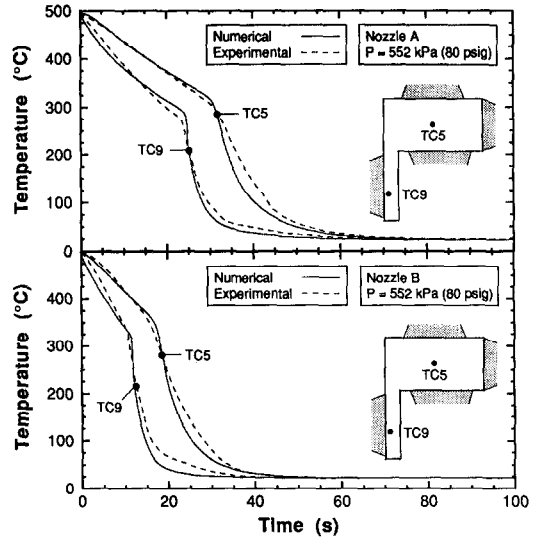

Fig. 11. Comparison of measured and predicted temperature–time envelopes of the L-shape.

history of the slowest cooling and fastest cooling thermocouples were presented so that the ability to predict accurately the temperature–time envelope was verified. Experimental measurements presented in a related study [22] confirmed that the hardness distribution of a heat treated part can be accurately predicted using the quench factor technique with the predicted thermal history. These confirmations pave the way for the final phase leading to the development of the CAD-based intelligent spray quenching system: incorporation of optimization routines, similar to the experimental steps performed in this study, into the finite element model so that the nozzle configuration can be selected prior to quenching.

CONCLUSIONS

This study continues the development of the CAD-based intelligent spray quenching system, originally proposed by Deiters and Mudawar [1], which, once completed, will optimize the quenching of aluminum alloys to achieve superior part quality. The primary goal of the present study was to develop a method capable of optimizing the mechanical properties of age-hardenable aluminum alloys. Key conclusions from this study are as follows.

(1) The dominant spray hydrodynamic parameter was identified using the spray quenching heat transfer correlations. The cooling rate in the film boiling regime can be increased by increasing the volumetric spray flux of the spray. This can be accomplished in two ways: (i) increase the operating pressure of the nozzles; or (ii) use a nozzle with a larger flow capacity. Both methods also increase the mean drop velocity which is also beneficial.

(2) Experiments were performed in which the initial nozzle configuration was selected based on the thermal mass distribution of the part. Subsequent quenches were improved by increasing the cooling rate of the slowest cooling regions of the part (or decreasing the cooling rate of the fastest cooling regions) such that the magnitude and uniformity of hardness (and yield strength) were maximized while maintaining a relatively thin temperature–time envelope (i.e. low residual stress). These experiments are identical to the steps the proposed intelligent spray quenching system would perform numerically in order to optimize the quench for an extrusion.

(3) The temperature–time envelope of a spray quenched part was successfully predicted using the spray quenching heat transfer correlations [18, 19] as boundary conditions within a finite element model. Thus, the mechanical properties of the part can be predicted without any experimental information. This numerical model represents the foundation of the intelligent spray quenching system. Once perfected, the performance of a spray quenching system can be judged prior to operation, thus significantly reducing cost and increasing productivity.

Acknowledgements—The authors gratefully acknowledge the financial support of the Purdue University Engineering Research Center for Intelligent Manufacturing Systems. Financial support for the first author was provided in the form of the United States Department of Energy Predoctoral Integrated Manufacturing Fellowship. The authors also thank Jerry Hagers, Rudolf Schick and Chris Schaffer of Spraying Systems Company for their valuable technical assistance.

REFERENCES

1. T. A. Deiters and I. Mudawar, Optimization of spray quenching for aluminum extrusion, forging, or continuous casting, *J. Heat Treating* **7**, 9–18 (1989).
2. J. C. Chevrier, A. Simon and G. Beck, Optimal cooling rate and process control in metallic parts heat treatment. In *Heat and Mass Transfer in Metallurgical Systems* (Edited by D. B. Spalding and N. H. Afgan), pp. 535–544. Hemisphere, Washington, DC (1981).
3. W. L. Fink and L. A. Willey, Quenching of 75S aluminum alloy, *Trans. AIME* **175**, 414–427 (1948).
4. J. S. Kim, R. C. Hoff and D. R. Gaskell, A quench factor analysis of the influence of water spray quenching on the age-hardenability of aluminum alloys, *Proceedings of the International Symposium on Materials Processing in the Computer Age*, pp. 203–221, New Orleans, LA (1991).
5. J. W. Evancho and J. T. Staley, Kinetics of precipitation in aluminum alloys during continuous cooling, *Metall. Trans.* **5**, 43–47 (1974).
6. J. T. Staley, Quench factor analysis of aluminum alloys, *Mater. Sci. Technol.* **3**, 923–935 (1987).
7. J. W. Cahn, Transformation kinetics during continuous cooling, *Acta Metall.* **4**, 572–575 (1956).
8. S. E. Axter, Effects of interrupted quenches on the properties of aluminum, CM80-409, Society of Manufacturing Engineers (1980).
9. American Society for Metals, *ASM Handbook* (10th Edn), Vol. 4. ASM International, Materials Park, Ohio (1991).
10. M. Conserva and P. Fiorini, Interpretation of quench-sensitivity in Al–Zn–Mg–Cu alloys, *Metall. Trans.* **4**, 857–862 (1973).
11. J. W. Evancho, Effects of quenching on strength and toughness of 6351 extrusions, 13-73-HQ40, Alcoa Laboratories, Alcoa Center, PA (1973).
12. R. R. Sawtell, Effects of quenching path in aluminum alloy 7075, *Aluminium* **60**, 198–202 (1984).
13. C. E. Bates, Selecting quenchants to maximize tensile properties and minimize distortion in aluminum parts, *J. Heat Treating* **5**, 27–40 (1987).
14. C. E. Bates and G. E. Totten, Procedure for quenching media selection to maximize tensile properties and minimize distortion in aluminum alloy parts, *Heat Treating*. **15**, 89–97 (1988).
15. C. E. Bates, Predicting properties and minimizing residual stress in quenched steel parts, *J. Heat Treating*. **6**, 27–45 (1988).
16. C. E. Bates and G. E. Totten, Application of quench factor analysis to predict hardness under laboratory and production conditions, *Proceedings of the First International Conference on Quenching and Control of Distortion*, pp. 33–39. Chicago, IL (1992).
17. D. P. DeWitt, Inferring temperature from optical radiation measurements, *Opt. Engng* **25**, 596–601 (1986).
18. W. P. Klinzing, J. C. Rozzi and I. Mudawar, Film and transition boiling correlations for quenching of hot surfaces with water sprays, *J. Heat Treating* **9**, 91–103 (1992).
19. I. Mudawar and W. S. Valentine, Determination of the local quench curve for spray-cooled metallic surfaces, *J. Heat Treating* **7**, 107–121 (1989).
20. D. D. Hall and I. Mudawar, Experimental and numerical study of quenching complex-shaped metallic alloys with multiple, overlapping sprays, *Int. J. Heat Mass Transfer* **38**, 1201–1216 (1995).
21. J. C. Rozzi, Quenching of aluminum parts having irregular geometries using multiple water sprays, M. S. Thesis, Purdue University, West Lafayette, IN (1991).
22. D. D. Hall and I. Mudawar, Predicting the impact of quenching on mechanical properties of complex-shaped aluminum alloy parts, *ASME J. Heat Transfer* **117**, 479–488 (1995).